International Journal of Biological Macromolecules 227 (2023) 925–937

Contents lists available at ScienceDirect

International Journal of Biological Macromolecules

journal homepage: www.elsevier.com/locate/ijbiomac

Onion-like doxorubicin-carrying polymeric nanomicelles with tumor acidity-sensitive dePEGylation to expose positively-charged chitosan shell for enhanced cancer chemotherapy

Shih-Yu Huang [a], Nien-Tzu Yeh [a], Tzu-Hao Wang [a], Tsai-Ching Hsu [b,c,d], Hao-Yang Chin [b], Bor-Show Tzang [b,c,d,e,*], Wen-Hsuan Chiang [a,**]

[a] Department of Chemical Engineering, National Chung Hsing University, Taichung 402, Taiwan
[b] Institute of Medicine, Chung Shan Medical University, Taichung 402, Taiwan
[c] Immunology Research Center, Chung Shan Medical University, Taichung 402, Taiwan
[d] Clinical Laboratory, Chung Shan Medical University Hospital, Taichung 402, Taiwan
[e] Department of Biochemistry, School of Medicine, Chung Shan Medical University, Taichung 402, Taiwan

ARTICLE INFO

Keywords:
Chitosan
Tumor acidity-responsive nanomicelles
dePEGylation

ABSTRACT

To effectively promote antitumor potency of doxorubicin (DOX), a regularly used chemotherapy drug, the tumor acidity-responsive polymeric nanomicelles from self-assembly of the as-synthesized amphiphilic benzoic imine-containing PEGylated chitosan-g-poly(lactic-co-glycolic acid) (PLGA) conjugates were developed as vehicles of DOX. The attained PEGylated chitosan-g-PLGA nanomicelles with high PEGylation degree (H-PEG-CSPNs) were characterized to exhibit a "onion-like" core-shell-corona structure consisting of a hydrophobic PLGA core covered by benzoic imine-rich chitosan shell and outer hydrophilic PEG corona. The DOX-carrying H-PEG-CSPNs (DOX@H-PEG-CSPNs) displayed robust colloidal stability under large-volume dilution condition and in a serum-containing aqueous solution of physiological salt concentration. Importantly, the DOX@H-PEG-CSPNs in weak acidic milieu undergoing the hydrolysis of benzoic imine bonds and increased protonation of chitosan shell showed dePEGylation and surface charge conversion. Also, the considerable swelling of protonated chitosan shell within DOX@H-PEG-CSPNs accelerated drug release. Notably, the cellular internalization of DOX@H-PEG-CSPNs by TRAMP-C1 prostate cancer cells under mimic acidic tumor microenvironment was efficiently boosted upon acidity-triggered detachment of PEG corona and exposure of positively-charged chitosan shell, thus augmenting DOX-mediated anticancer effect. Compared to free DOX molecules, the DOX@H-PEG-CSPNs appreciably suppressed TRAMP-C1 tumor growth in vivo, thereby showing great promise in improving DOX chemotherapy.

1. Introduction

In the past two decades, the chemotherapy has been frequently adopted in the clinical cancer treatment [1–6]. Nevertheless, chemotherapy drugs that are usually non-specific small molecules have poor pharmacokinetic profiles and easily accumulate in normal tissues and organs, thus not only eliciting serious side effects (such as bone marrow suppression, cardiomyopathy, nephrotoxicity, neurotoxicity and multi-drug resistance) but also reducing therapeutic efficacy [6–8]. These drawbacks largely restrict the clinical use of cancer chemotherapy. To effectively improve cancer chemotherapy, it is essential to develop a drug delivery system capable of changing chemotherapeutic drug biodistribution, promoting drug accumulation in the tumor regions and decreasing drug adverse effect [6–12]. In this end, taking advantages of the inherent enhanced permeability and retention (EPR) effect of solid tumor, recently, a varied of nanoparticles such as liposomes [13,14], polymeric micelles [15–17], solid-lipid nanoparticles [18,19] and metal-organic frameworks (MOF) [1,20,21] have been created as vehicles for tumor-targeted drug delivery. However, after being administered intravenously, these drug-carrying nanoparticles as an invader frequently are recognized by the native immunity system, thus being engulfed by the macrophages-rich reticuloendothelial system (RES)

* Correspondence to: B.-S. Tzang, Institute of Medicine, Chung Shan Medical University, Taichung 402, Taiwan.
** Corresponding author.
E-mail addresses: bstzang@csmu.edu.tw (B.-S. Tzang), whchiang@dragon.nchu.edu.tw (W.-H. Chiang).

https://doi.org/10.1016/j.ijbiomac.2022.12.172
Received 24 October 2022; Received in revised form 30 November 2022; Accepted 16 December 2022
Available online 20 December 2022

[22]. In this case, the therapeutic nanoparticles will be largely eliminated from the blood circulation system and reduce their accumulation within tumor sites, thereby giving rise to the reduced antitumor potency and increased side effect.

To overcome these challenges, the most common strategy of prolonging the blood circulation time of nanoparticles is surface decoration by hydrophilic poly(ethylene glycol) (PEG), which is well-known as PEGylation [23–26]. Several research groups have demonstrated that the PEGylation of nanoparticles can effectively reduce their removal by the RES, thus prolonging their blood circulation and promoting their accumulation in tumor sites [23–26]. Despite this, the lately increased studies pointed out that these PEG-coated nanoparticles showed the poor cellular uptake due to steric repulsion of PEG-rich surfaces, thus diminishing intracellular drug delivery and efficacy of tumor treatment [23,27,28]. In order to address the aforementioned "PEG dilemma", some tactics to fabricate the functionalized nanoparticles capable of dissociating PEG layer (considered as dePEGylation) in response to acidic tumor microenvironment (pH_e 6.5–7.0) and tumor extracellular matrix have been reported [27–31]. For example, Jiang et al. synthesized pH_e-responsive PEG-pH_e-poly(L-glutamic acid) (PLG) and matrix metalloproteinases-2/9 (MMP-2/9) (MMP)-sensitive PEG-MMP-PLG by using pH_e-responsive cleavage 2-propionic-3-methylmaleic anhydride (CDM)-derived amide bond and matrix MMP-sensitive degradable peptide PLGLAG to link PLG and PEG [29]. Through the complexation of polypeptides and cisplatin (CDDP), the corresponding PEG-pH_e-PLG-Pt and PEG-MMP-PLG-Pt nanoparticles were then attained. After arriving tumor tissue, these CDDP-loaded nanoparticles detached the PEG shielding as triggered by pH_e or MMP, thereby enhancing intratumoral CDDP retention, boosting cell internalization, and promoting antitumor efficacy on a fatal high-grade serous ovarian cancer mouse model. Moreover, as reported by Cui's group [30], to promote intracellular delivery of zoledronic acid (ZA), a third generation bisphosphonate, the ZA/calcium complex-encapsulated poly(lactic-*co*-glycolic acid) (PLGA) nanoparticles stabilized with octadecanoic acid-hydrazone-PEG were developed. Through the PEG detachment due to tumor acidity-induced hydrolysis of hydrazone bonds, the ZA-carrying nanoparticles considerably reduced the distribution of ZA in bones and augmented its accumulation in extraskeletal tumors in vivo, thus significantly boosting antitumor efficacy.

On the other hand, in addition to the aforementioned dePEGylation, the exposed positively-charged surface of nanoparticles once deposited in the tumor microenvironment has been demonstrated to remarkably enhance their internalization by cancer cells via electrostatic attraction, thus increasing tumor uptake [7,32–34]. For instance, Chen and *co*-workers developed a polyprodrug-based nanomedicine with zwitterionic-to-cationic charge conversion capability (denoted as ZTC-NMs) for enhanced chemotherapeutic drug delivery [7]. The ZTC-NMs composed of the pH-responsive poly(carboxybetaine)-like zwitterionic segments and glutathione-responsive camptothecin prodrug segments can expose the surface positive charges in response to acidic tumor microenvironment, thus promoting cellular internalization efficiency of the nanomedicines to inhibit in vivo tumor growth in an effective manner. Furthermore, as shown in our previous work [34], the designed nanovehicles comprising hydrophobic PLGA cores coated with pH-responsive *N*-acetyl histidine modified D-α-tocopheryl polyethylene glycol succinate (NAcHis-TPGS) not only switched surface charges in response to tumor extracellular acidity but also selectively co-delivered indocyanine green (ICG), a photothermal agent, and doxorubicin (DOX), a chemotherapy drug, to tumor sites. Taking advantage of the small size in combination with the increase in surface positive charges upon the pH_e-elicited protonation of NAcHis residues, the cargo-carrying nanoparticles considerably accumulated in acidic tumor sites in vivo and penetrated into the deep tumor hypoxia regions upon the enhanced internalization by both TRAMP-C1 cancer cells and tumor-associated macrophages, thereby leading to extensive tumor tissue/vessel ablation by photothermal/chemo combinatorial therapy.

In view of the above pioneer studies, we rationally presumed that the tailor-made nanoparticles engineered with tumor site-specific dePEGylation in combination with positively-charged surface could further boost their uptake by cancer cells and antitumor potency. In order to prove our assumption, a practical strategy was utilized in this study to fabricate the tumor acidity-responsive polymeric nanomicelles capable of transporting DOX to tumor tissues and then detaching PEG shielding to expose positively-charged surfaces (Scheme 1). Besides, this is particularly important that the biodegradable and biocompatible materials are used in developing nanoparticle-based drug delivery systems, a critical prerequisite for the clinical cancer treatment. Considering that chitosan exhibits biocompatibility, biodegradability, mucoadhesive, amine-rich and acidity-triggered protonation properties [15,35,36], while the PLGA, a biocompatible and biodegradable polymer, has been approved by the United States Food and Drug Administration for clinical use [37,38], in this work, by the conjugation of chitosan with carboxylic acid-terminated PLGA via amindation, the chitosan-*g*-PLGA adduct was attained and utilized as important component of the polymeric nanomicelles. Subsequently, the benzoic imine-containing PEGylated chitosan-g-PLGA conjugates were obtained by the coupling of chitosan-g-PLGA with methoxy PEG benzaldehyde (mPEG-CHO) via Schiff base reaction. Through the self-assembly of amphiphilic PEGylated chitosan-g-PLGA adducts in an aqueous solution of pH 8.5, the PEGylated chitosan-g-PLGA nanomicelles with high PEGylation degree (denoted as H-PEG-CSPNs) were fabricated. The H-PEG-CSPNs were characterized to have a "onion-like" core-shell-corona structure composed of a hydrophobic PLGA core surrounded by benzoic imine-rich chitosan interfacial shell and outer hydrophilic PEG corona. Moreover, the H-PEG-CSPNs showed prominent colloidal stability in a serum-containing aqueous solution of physiological salt concentration. By the π-π stacking and hydrophobic interactions of DOX molecules and H-PEG-CSPNs, the attained DOX-loaded H-PEG-CSPNs (DOX@H-PEG-CSPNs) showed the dePEGylation and surface charge conversion in response to acidic environment due to cleavage of benzoic imine bonds and increased protonation of chitosan shell. Also, the significant swelling of protonated chitosan shell within DOX@H-PEG-CSPNs under acidic condition enhanced drug outflow. Notably, the DOX@H-PEG-CSPNs were efficiently internalized by TRAMP-C1 prostate cancer cells in mimic tumor acidic milieu upon acidity-triggered detachment of PEG corona and exposure of positively-charged chitosan shell, thus promoting DOX-mediated anticancer effect. The in vivo tumor growth inhibition study further revealed that the DOX@H-PEG-CSPNs exhibited the capability of suppressing TRAMP-C1 tumor growth superior to free DOX molecules, proving the great potential in cancer treatment.

2. Experimental section

2.1. Materials

DOX (in the hydrochloride salt form) was purchased from Carbosynth Ltd. (UK). PLGA (lactide: glycolide = 75:25, MW 10 kDa, inherent viscosity: 0.11 dL/g, acid-terminated) was acquired from Green Square (Taiwan). Chitosan oligosaccharide (MW 5.0 kDa, 81 % degree of deacetylation) were attained from Glentham Life Science Ltd. (UK). mPEG-CHO (MW 5.0 kDa) used in this study was synthesized by our previous work [39]. Dimethyl sulfoxide (DMSO) was obtained from Echo Chemical Co., Ltd. (Taiwan). Dulbecco's modified Eagle medium (DMEM), propidium (PI, 94 %), 3-(4,5-Dimethylthiazol-2-yl)-2,5-diphenyltetrazolium bromide (MTT), D_2O (99.9 atom % D) and DMSO-d_6 (99.8 atom % D) were purchased from Sigma-Aldrich (USA). N-(3-Dimethylaminopropyl)-N′-ethylcarbodiimide hydrochloride (EDC, 95 %) was attained from Matrix Scientific (USA). N-hydroxysuccinimide (NHS, 98 %) was acquired from Alfa Aesar (USA). Fetal bovine serum (FBS) was purchased from Hyclone (USA). Hoechst 33342 was

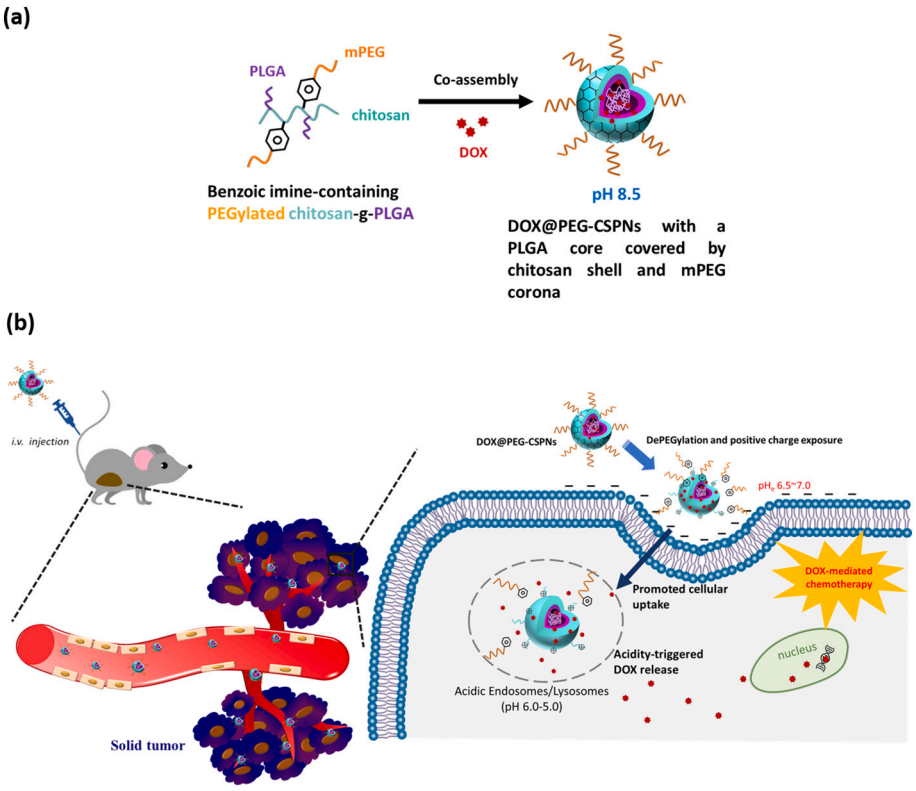

Scheme 1. Illustration of (a) preparation of DOX@PEG-CSPNs and (b) tumor acidity-elicited dePEGylation and positive-charged surface exposure of DOX@PEG-CSPNs to enhance intracellular DOX delivery and cancer chemotherapy.

purchased from Invitrogen. Calcein-AM was obtained from AAT Bioquest (USA). Deionized water was produced from Milli-Q Synthesis (18 MΩ, Millipore). All other chemicals were reagent grade and used as received. TRAMP-C1 cells (murine prostate cancer cell line) and 4T1 cells (murine breast cancer cell line) were acquired from Food Industry Research and Development Institute (Hsinchu City, Taiwan).

2.2. Synthesis and characterization of chitosan-g-PLGA adducts

The chitosan-g-PLGA adducts was synthesized by the amide-linkage-based conjugation of amine groups of chitosan with carboxylic acid end of PLGA (Scheme 2). Briefly, chitosan (20 mg), PLGA (118.4 mg), NHS (40.9 mg) and EDC hydrochloride (68.1 mg) were dissolved in DMSO

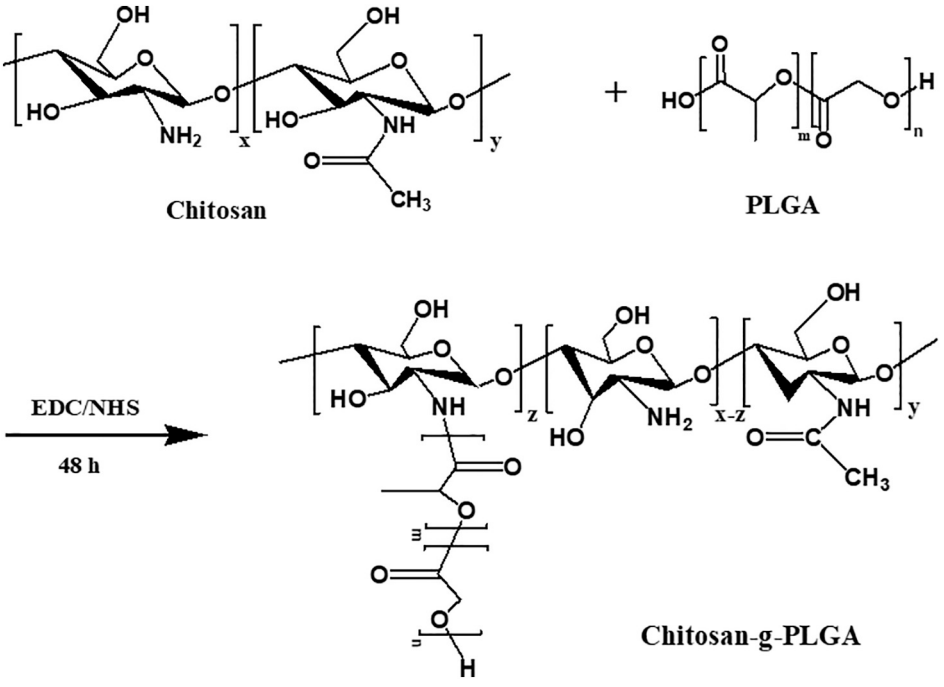

Scheme 2. Synthetic route and chemical structure of chitosan-g-PLGA adducts.

(1.0 mL). Subsequently, the solution was stirred at room temperature for 48 h and dialyzed (Cellu Sep MWCO 6000–8000) against deionized water to remove NHS and EDC. The final product was obtained by freeze drying. The chemical composition of chitosan-g-PLGA adducts were characterized by Fourier transform infrared (FT-IR) spectroscopy (FT-720, HORIBA, Japan) using KBr pellet for the sample preparation, proton nuclear magnetic resonance (^{1}H NMR) spectroscopy (Agilent DD2 600 MHz NMR spectrometer) using DMSO-d_6 as the solvent. Furthermore, to obtain the weight ratio of chitosan and PLGA in chitosan-g-PLGA adducts, thermogravimetric analysis (TGA) was conducted with thermogravimetric analyzer EXSTAR TG/DTA 6200 (Seiko Instruments Inc) in an N_2 atmosphere upon heating the sample to 800 °C at the rate of 10 °C/min.

2.3. Preparation of PEGylated chitosan-g-PLGA nanomicelles (PEG-CSPNs)

The PEG-CSPNs with high PEGylation degree (denoted as H-PEG-CSPNs) were prepared by one-step nanoprecipitation method. Briefly, the chitosan-g-PLGA (6.0 mg) and mPEG-CHO (4.0 mg) were completely dissolved in DMSO (0.4 mL). The solution was gently stirred at room temperature for 16 h to attain the benzoic imine-containing PEGylated chitosan-g-PLGA conjugates, followed by dropwise addition into pH 8.5 phosphate buffer (ionic strength 0.01 M, 1.6 mL) under stirring. The mixture was stirred at room temperature for 2 h and then dialyzed (Cellu Sep MWCO 6000–8000) against pH 8.5 phosphate buffer at 4 °C to attain the H-PEG-CSPNs. It should be mentioned that the pH 8.5 phosphate buffer was used in dialysis procedure to avoid hydrolysis of benzoic imine bonds within H-PEG-CSPNs. For comparison, the same concentration (3.0 mg/mL) of chitosan-g-PLGA conjugates was adopted to prepare the non-PEGylated CSPNs in a similar manner. On the other hand, the pristine PLGA nanoparticles (PNs) (PLGA concentration = 2.0 mg/mL) were also attained by the aforementioned approach.

2.4. Preparation of DOX@H-PEG-CSPNs

The DOX@H-PEG-CSPNs were prepared by the single-step nanoprecipitation method. Briefly, the chitosan-g-PLGA (6.0 mg) and mPEG-CHO (4.0 mg) were completely dissolved in DMSO (0.3 mL) and the solution was stirred at room temperature for 16 h to obtain the PEGylated chitosan-g-PLGA adducts. Next, DOX (1.0 mg) dissolved in DMSO (0.1 mL) was added to the above solution. The mixture was added dropwise into pH 8.5 phosphate buffer (1.6 mL) and stirred at room temperature for 2 h, followed by dialysis (Cellu Sep MWCO 6000–8000) against pH 8.5 phosphate buffer at 4 °C for 24 h to remove DMSO and unloaded DOX. For comparison, the DOX@L-PEG-CSPNs with low PEGylation degree ([mPEG-CHO]/[chitosan-g-PLGA] = 1/6 (*w*/w)) were fabricated in a similar approach. Furthermore, to explore the effect of benzoic imine-involved PEGylation on the colloidal stability of DOX-loaded assemblies, the DOX/chitosan-g-PLGA/mPEG-CHO assemblies, DOX/chitosan-g-PLGA assemblies, and DOX/PLGA/mPEG-CHO assemblies were attained by simple mixing. For example, for the preparation of DOX/chitosan-g-PLGA/mPEG-CHO assemblies, the chitosan-g-PLGA adducts (6.0 mg) and mPEG-CHO (4.0 mg) were simply mixed in DMSO (0.3 mL). Subsequently, DOX (1.0 mg) dissolved in DMSO (0.1 mL) was added to the above solution and the resulting solution was stirred at room temperature for 2 h and dialyzed by the aforementioned approach. The DOX/chitosan-g-PLGA assemblies and DOX/PLGA/mPEG-CHO assemblies were fabricated in a similar way.

2.5. Structural characterization

The mean hydrodynamic diameter (D_h) and particle size distribution of pristine PLGA nanoparticles, CSPNs, H-PEG-CSPNs, DOX@H-PEG-CSPNs and DOX@L-PEG-CSPNs in aqueous solutions were determined with a Brookhaven BI-200SM goniometer equipped with a BI-9000 AT digital correlator using a solid-state laser (35 mW, $\lambda = 637$ nm) detected at a scattering angle of 90°. The zeta potential of the above nanoparticles in aqueous solutions was measured by a Litesizer 500 (Anton Paar, USA). At least triplicate measurements of each sample were conducted and then averaged. To explore the morphology of polymeric assemblies in aqueous solutions at pH 7.4 and 5.5, respectively, the angular dependence of autocorrelation functions of H-PEG-CSPNs and DOX@H-PEG-CSPNs and their R_g/R_h ratio of the root-mean-square radius of gyration (R_g) to the mean hydrodynamic radius (R_h) were attained by dynamic and static light scattering (DLS/SLS) measurements using a Brookhaven BI-200SM goniometer. Based on the Berry plot of the scattering intensity ($I_{ex}^{-1/2}$) versus the square of the scattering vector (q^2) from the angle-dependent measurements of the light scattering intensity, the R_g of these nanoparticles was quantitatively determined. The UV/Vis spectra of mPEG-CHO, CSPNs and H-PEG-CSPNs in 0.15 M phosphate buffered saline (PBS) of pH 7.4 were acquired using a UV/Vis spectrophotometer (V-730, JASCO, United States). Transmission electron microscopy (TEM) images of CSPNs, H-PEG-CSPNs and DOX@H-PEG-CSPNs negatively stained with phosphotungstic acid hydrate (2.0 wt%) were obtained from a JEOL JEM-1400 CXII microscope. The fluorescence spectra of H-PEG-CSPNs, DOX@H-PEG-CSPNs and free DOX molecules in pH 7.4 PBS were attained using a Hitachi F-2700 fluorescence spectrometer. Furthermore, in order to further confirm the acidity-triggered hydrolysis of benzoic imine bonds within H-PEG-CSPNs, the H-PEG-CSPNs were dispersed in pH 6.5 aqueous solution and then stirred at 37 °C for 24 h. Afterward, the acidity-treated H-PEG-CSPNs were lyophilized and characterized by ^{1}H NMR spectroscopy.

2.6. DOX loading efficiency and content

To quantify the amount of DOX loaded within nanomicelles, a preset volume (50 μL) of the DOX@PEG-CSPN solutions was lyophilized and dissolved in DMSO to disrupt micelles for drug extraction. The excitation was performed at 480 nm and the DOX fluorescence in the range 500–700 nm was measured by a Hitachi F-2700 fluorescence spectrometer. The calibration curve used for drug loading characterization was attained by fluorescence intensity of DOX with various concentrations in DMSO. The loading efficiency (LE) and loading content (LC) of DOX were calculated by the following formulas:

$$\text{LE}\ (\%) = (\text{weight of loaded DOX}/\text{weight of DOX in feed}) \times 100\%$$

$$\text{LC}\ (\%) = (\text{weight of loaded DOX}/\text{total weight of the DOX} - \text{loaded nanomicelles}) \times 100\%$$

2.7. In vitro DOX release performance

To study in vitro DOX liberation behavior of DOX@H-PEG-CSPNs and DOX@L-PEG-CSPNs, the aqueous solutions (1.0 mL) of the DOX-carrying nanomicelles was dialyzed (Cellu Sep MWCO 6000–8000) against PBS (pH 7.4, 0.15 M) and acetate buffer (pH 5.0 and 4.0, 0.15 M) (25 mL) at 37 °C, respectively, under gentle shaking (100 rpm). At the different time intervals, 1.0 mL of the dialysate was taken out for analysis and replaced with an equal volume of fresh buffer. The amount of DOX released was determined by fluorescence measurements as described above.

2.8. In vitro cellular uptake

Free DOX molecules, DOX@H-PEG-CSPNs and DOX@L-PEG-CSPNs were separately dispersed in DMEM of pH 7.4 and 6.5 to a DOX concentration of 10 μM. TRAMP-C1 cells (2×10^5 cells/well) seeded onto 22 mm round glass coverslips in 6-well plates were incubated with the above solutions at 37 °C for 1 and 4 h. After being washed twice with HBSS and immobilized with 4 % formaldehyde, the cell nuclei were stained with Hoechst 33342. The cellular images were obtained using a

confocal laser scanning microscope (CLSM) (Olympus, FluoView FV3000, Japan) equipped with a Hoechst set (Ex. 405 nm) and a DOX set (Ex. 488 nm). Also, the cellular internalization of DOX@H-PEG-CSPNs and DOX@L-PEG-CSPNs (DOX concentration = 10 μM) by TRAMP-C1 cells at 37 °C and at pH 7.4 and 6.5 was evaluated by a FACSCalibur flow cytometer (BD Bioscience). After 1 and 4 h incubation, the treated TRAMP-C1 cells (3×10^5 cells/well) were detached with trypsine-EDTA solution and then dispersed in PBS (1.0 mL). A minimum of 1×10^4 cells were analyzed from each batch with fluorescence intensity displayed on a log scale.

2.9. In vitro cytotoxicity

TRAMP-C1 cells at a density of 1×10^4 cells/well were seeded in a 96-well plate and incubated with DMEM containing 10 % FBS and 1 % penicillin at 37 °C for 24 h. The medium was then replaced with 100 μL of fresh medium (pH 7.4 or 6.5) containing free DOX molecules or DOX-carrying nanomicelles at various DOX concentrations or drug-free H-PEG-CSPNs, and cells were incubated at 37 °C for additional 24 h. Subsequently, 100 μL MTT (0.25 mg/mL) was added into each well and then incubated at 37 °C for 3 h. After discarding the culture medium, 120 μL DMSO was added into each well to dissolve the precipitate and the absorbance of the resulting solution at 570 nm was measured using a BioTek 800TS microplate reader. Besides, the cytotoxicity of free DOX molecules and DOX@H-PEG-CSPNs on 4 T1 cells was assessed in a similar manner. On the other hand, the anticancer effect of DOX@H-PEG-CSPNs on TRAMP-C1 cells was assessed by fluorescence staining of live/dead cells. TRAMP-C1 cells (1.5×10^5 cells/well) were seeded in a 12-well plate and incubated at 37 °C for 24 h in DMEM containing 10 % FBS and 1 % penicillin. The medium was then replaced with 1.0 mL of fresh medium containing DOX@H-PEG-CSPNs was incubated at pH 7.4 and 6.5 for additional 24 h. Next, cells were gently washed with PBS twice to avoid washing off dead cells. Calcein AM (0.2 μM) and PI (25 μg/mL) mixture solution (500 μL) was added and kept at room temperature for 30 min. The cellular images were acquired using a NIB-100F inverted fluorescent biological microscope (Nanjing Jiangnan Novel Optics Co., Ltd., China).

2.10. In vivo tumor growth inhibition

Male C57BL/6 J mice (5–6 weeks old), purchased from National Laboratory Animal Center (Taiwan), were cared based on the Guidance Suggestions for the Care and Use of Laboratory Animals, approved by the Administrative Committee on Animal Research in the Chung Shan Medical University (Taiwan) (IACUC Approval No: 2719). 8×10^6 TRAMP-C1 cells were subcutaneously injected into the right thigh of mice to establish tumor model. Tumor volume (V) was calculated as follows: $V = L \times W^2/2$, where L the tumor dimension at the longest point and W is the tumor measurement at the widest point. When tumor volume of the mice enlarged to 80–100 mm^3, the TRAMP-C1 tumor-bearing mice were randomly divided into 4 groups (4 in each group) and intravenous (i.v.) injected with PBS, free DOX molecules, DOX@H-PEG-CSPNs and DOX@L-PEG-CSPNs at a DOX dosage of 1.2 mg/kg, respectively. Each group was treated with a total of two doses at days 0 and 2. Tumor volume and body weight of mice were measured every 2 days until 18 days post-injection. To assess the antitumor efficacy, the relative tumor volumes (V/V_o) were obtained by the normalization of the tumor volumes (V) against the original volumes (V_o). After treatment, the TRAMP-C1 tumor-bearing mice were sacrificed by CO_2 euthanasia and the tumors were then isolated and weighted for therapeutic index (TI) measurements. The TI defined below was employed as a quantitative measure of therapeutic efficacy.

$$\mathrm{TI}\ (\%) = \left(1 - \frac{\text{Weight of tumor in the experimental group}}{\text{Weight of tumor in the control group}}\right) \times 100\%$$

On the other hand, the mice organs, including heart, liver, spleen, lung, kidney, and xenograft tumor, were excised and fixed with 10 % formalin, followed by embedment with paraffin wax. The embedded tissues were sectioned in to 5 mm for hematoxylin and eosin (H&E) staining and Ki67 immunohistochemical staining. Sections of tumors and major organs of pertinent sizes were stained with H&E and Ki67, and examined by an Olympus IX70 inverted microscope (Japan).

2.11. Statistical analysis

All data are presented as the mean ± standard deviation (SD). The difference among groups were evaluated using one-way or two-way ANOVA analysis. Statistical significance is indicated as (ns) $P > 0.05$, (*) $P < 0.05$, (**) $P < 0.01$ and (***) $P < 0.001$.

3. Results and discussion

3.1. Synthesis and characterization of chitosan-g-PLGA and PEG-CHO

The chitosan-g-PLGA adduct used in this work was synthesized by the coupling of chitosan oligosaccharide with acid-terminated PLGA upon NHS/EDC-mediated amindation and characterized by FT-IR and ^{1}H NMR measurements. As presented in the FT-IR spectrum of chitosan-g-PLGA adducts (Fig. 1), in addition to the feature absorption bands of C═O stretching vibration of PLGA at 1751 cm^{-1}, the absorption bands at 1110 and 2891 cm^{-1} for C—O and C—H stretching vibration, respectively, and at 1623 and 1531 cm^{-1} for C═O stretching vibration and N—H bending vibration of amide groups, respectively, from chitosan were observed. Moreover, in the ^{1}H NMR spectrum of chitosan-g-PLGA (Fig. 2), the appearance of the feature proton signals of PLGA at δ 4.9 and 5.2 ppm, respectively, and of chitosan at δ 2.0 and 2.8 ppm, respectively, was attained. These findings evidently indicate the successful conjugation of chitosan with PLGA. Furthermore, as revealed in the TGA profiles (Fig. S1), the chitosan-g-PLGA adducts consist of ca 23.5 wt% chitosan and 76.5 wt% PLGA. As a result, the degree of substitution of chitosan with PLGA defined as the number of PLGA segments per 100 glucosamine units was obtained to be ca 5.5. On the other hand, the PEG-CHO utilized in this work was attained according to our previous studies [39]. Based on signal integral ratio of the methoxy protons (δ 3.5 ppm) and aldehyde protons (δ 10.1 ppm) in the ^{1}H NMR spectrum of mPEG-CHO (Fig. 2), beyond 97 % of end hydroxyl group of mPEG was converted into aldehyde group.

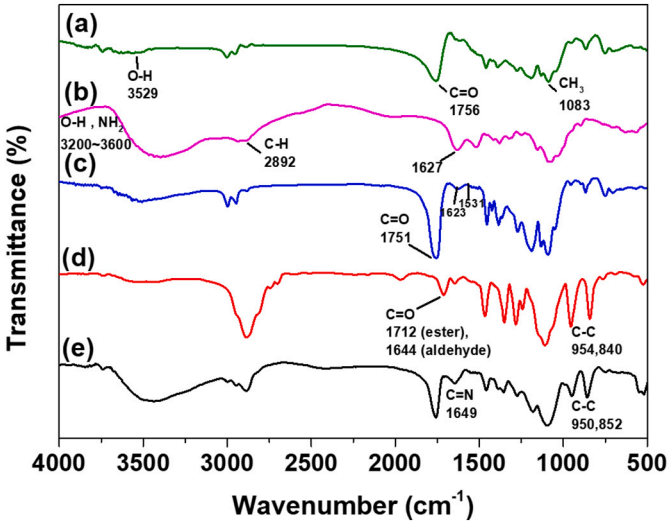

Fig. 1. FT-IR spectra of (a) PLGA, (b) chitosan, (c) chitosan-g-PLGA, (d) mPEG-CHO and (e) PEGylated chitosan-g-PLGA.

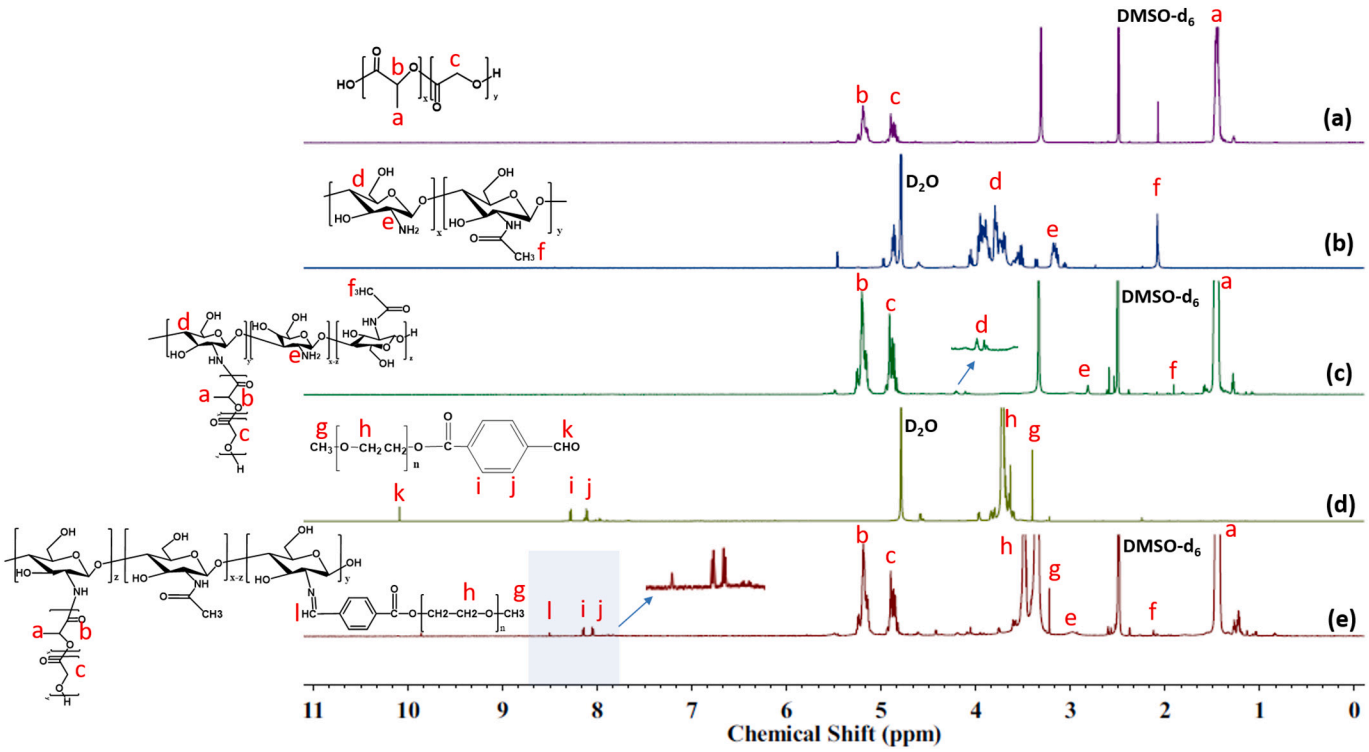

Fig. 2. [1]H NMR spectra of (a) PLGA, (b) chitosan, (c) chitosan-g-PLGA, (d) mPEG-CHO and (e) PEGylated chitosan-g-PLGA.

3.2. Preparation and characterization of CSPNs and PEG-CSPNs

Due to the hydrophobic nature of PLGA segments and the hydrophilic property of chitosan oligosaccharide, it was expected that the resulting chitosan-g-PLGA adducts could show an amphiphilic character in aqueous solution. Through the one-step nanoprecipitation approach, PLGA segments and chitosan-g-PLGA adducts in aqueous phase tended to self-assembly into PNs and CSPNs, respectively. As presented in Fig. 3a and Table 1, the mean D_h of PNs and CSPNs in pH 7.4 PBS was determined by DLS to be ca 74.7 nm and 174 nm, respectively. Obviously, compared to linear PLGA segments, the graft-type chitosan-g-PLGA adducts in aqueous phase were apt to associate into relatively

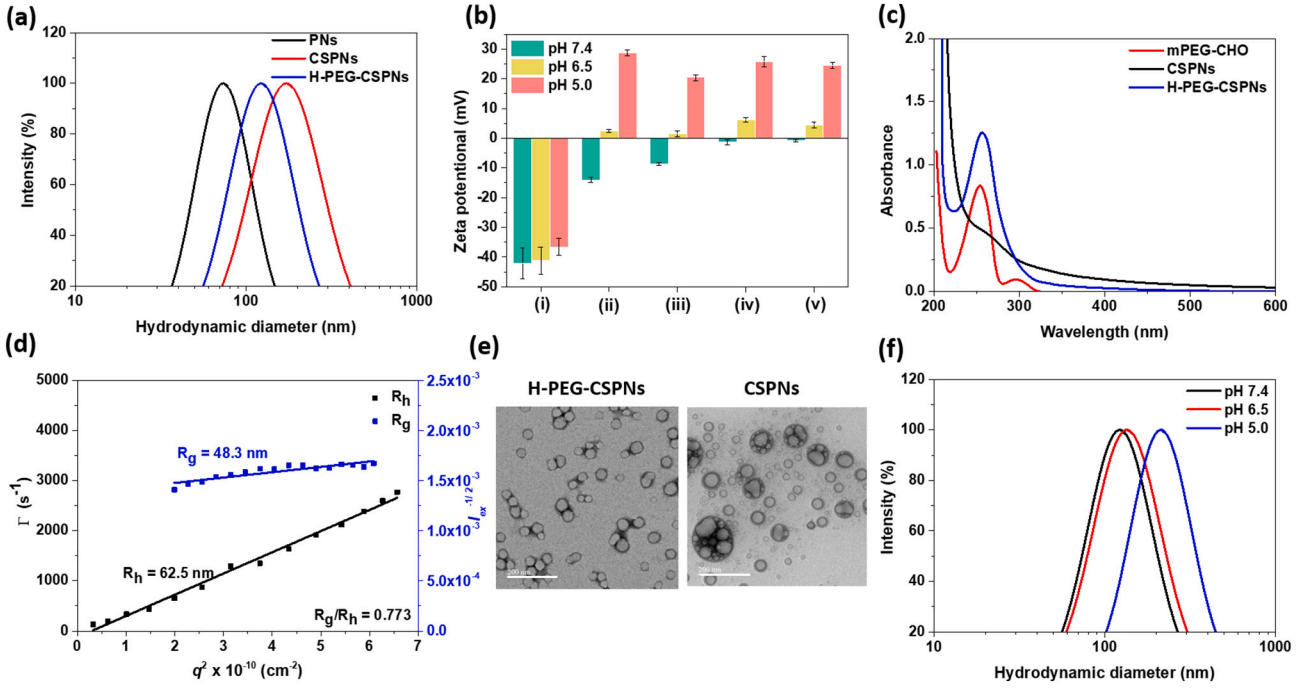

Fig. 3. (a) DLS size distribution profiles of PNs, CSPNs and H-PEG-CSPNs in pH 7.4 PBS. (b) Zeta potential of (i) PNs, (ii) CSPNs, (iii) H-PEG-CSPNs, (iv) DOX@H-PEG-CSPNs and (v) DOX@L-PEG-CSPNs in aqueous solutions at different pH. (c) UV/Vis spectra of mPEG-CHO, CSPNs and H-PEG-CSPNs in pH 7.4 PBS. (d) Berry plot for R_g and angle dependent correlation function of R_h of H-PEG-CSPNs in pH 7.4 PBS. (e) TEM images of H-PEG-CSPNs and CSPNs. Scale bars are 200 nm. (f) DLS size distribution profiles of H-PEG-CSPNs in aqueous solutions of different pH.

Table 1
DLS characteristics and drug loading capacities of various nanoassemblies.

Sample	D_h (nm)	PDI	LE (%)	LC (wt%)
PNs	74.7 ± 1.6	0.22 ± 0.01	–	–
CSPNs	174.0 ± 2.6	0.26 ± 0.03	–	–
H-PEG-CSPNs	131.8 ± 7.2	0.27 ± 0.03	–	–
DOX@H-PEG-CSPNs	137.8 ± 1.9	0.26 ± 0.01	76.5 ± 0.8	7.1 ± 0.1
DOX@L-PEG-CSPNs	162.3 ± 7.3	0.22 ± 0.06	62.5 ± 1.6	8.2 ± 0.2

large nanoassemblies. Moreover, Fig. 3b revealed that the zeta potential (ca −42.3 mV) of PNs in aqueous solution of pH 7.4 was considerably higher than that (−15.1 mV) of CSPNs under the same condition. This could be attributed to that the considerable dissociation of carboxylic acid groups in the end of PLGA segments rendered the surfaces of PNs appreciably negatively charged. By contrast, the negative charges on the surfaces of CSPNs were largely reduced because the carboxylic acid groups of PLGA segments were effectively conjugated with amine residues of chitosan. Notably, with the medium pH being adjusted from 7.4 to 5.0, distinct from the nearly unchanged zeta potential of PNs, the dramatic conversions in zeta potential of CSPNs from slightly negative to markedly positive values were observed. This strongly suggests that the acidity-elicited protonation of amine groups on the chitosan-rich surfaces of CSPNs profoundly increases the surface positive charges. On the other hand, compared to the markedly enlarged particle size of PNs in 10 % FBS-containing PBS over 1 h due to their massive aggregation, the well-dispersed colloidal stability of CSPNs in the same milieu was attained (Fig. S2), signifying that their hydrophilic chitosan-covered surfaces could prevent inter-particle aggregation in the serum-containing environment.

In order to prolong the blood circulation of nanoparticle-based drug delivery systems by reducing their fast clearance by RES, the PEGylation of nanoparticles has been frequently adopted. In this study, at the different mass ratios of mPEG-CHO to chitosan-g-PLGA, the mPEG-CHO segments were covalently conjugated with chitosan-g-PLGA adducts upon Schiff base reaction. The resulting PEGylated chitosan-g-PLGA adduct ([mPEG-CHO]/[chitosan-g-PLGA] = 2/3 (*w*/w)) was characterized by FT-IR and ^{1}H NMR. As shown in Fig. 1, in addition to the feature absorption bands of chitosan-g-PLGA adducts, the absorption bands at 1110 and 950/852 cm^{-1} for C—O and C—C stretching vibration of mPEG segments, respectively, and at 1649 cm^{-1} for C═N stretching vibration were observed in the FT-IR spectrum of PEGylated chitosan-g-PLGA adducts. Furthermore, in addition to feature proton signals of chitosan-g-PLGA adducts, the proton signals of ethylene and methoxy groups of mPEG at δ 3.5 and 3.2 ppm, respectively, and of benzene ring and imine groups at δ 8.0–8.2 and 8.5 ppm, respectively, appeared in the ^{1}H NMR spectrum of PEGylated chitosan-g-PLGA adducts (Fig. 2e). Note that, different from the single thermal decomposition temperature of chitosan-g-PLGA adducts and mPEG-CHO segments attained by TGA measurement (Fig. S1), two thermal decomposition temperatures of PEGylated chitosan-g-PLGA adducts at ca 260 and 350 °C, respectively, were observed. These results strongly confirm the successful conjugation of mPEG-CHO with chitosan-g-PLGA via the formation of benzoic imine bonds. Next, the H-PEG-CSPNs were fabricated through the self-assembly of the above PEGylated chitosan-g-PLGA adducts in an aqueous solution of pH 8.5. Different from CSPNs without significant absorption peak (Fig. 3c), the H-PEG-CSPNs showed the characteristic absorption peak (ca 260 nm) of benzene ring from benzoic imine bonds between chitosan and mPEG. In view of highly hydrated capability of mPEG segments, it was presumed that the hydrophilic mPEG segments tended to reside on the surfaces of H-PEG-CSPNs to stabilize the colloidal structure. Due to the presence of mPEG-rich hydrophilic layer, the H-PEG-CSPNs exhibited smaller particle size and lower zeta potential as compared to CSPNs as presented in Fig. 3a and b. To get insight into structural characteristics of H-PEG-CSPNs in pH 7.4 PBS, the variable angle SLS/DLS measurements and TEM observation were performed. Notably, a linear correlation between the relaxation frequency and the square of the scattering vector was observed in the angle-dependent DLS data of H-PEG-CSPNs (Fig. 3d). This suggests that the H-PEG-CSPNs dispersed in aqueous phase possess a spherical shape. Also, the TEM images of H-PEG-CSPNs revealed their well-dispersed spherical particle form (Fig. 3e). According to the Berry plot of $I_{ex}^{-1/2}$ versus q^2 from SLS examination, the R_g value of H-PEG-CSPNs was also obtained to be ca 48.3 nm. For H-PEG-CSPNs, the calculated R_g/R_h ratio (ca 0.773) is identical to that (0.77) of solid sphere-like nanoparticles as reported elsewhere [40,41]. Based on the angle-dependent SLS/DLS results and TEM images, and the superior hydration and steric repulsion effect of mPEG segments [42,43], it was confirmed that the amphiphilic PEGylated chitosan-g-PLGA adducts were apt to self-assemble into well-dispersed H-PEG-CSPNs with a spherical core-shell-corona hierarchical architecture composed of a solid PLGA core covered by intermediate chitosan shell and outer mPEG corona, whereas, in the lack of hydrophilic mPEG segments, the chitosan-g-PLGA adducts undergoing self-assembly tended to form CSPNs with multicore-like aggregation structure as shown in the TEM images (Fig. 3e).

Notably, in comparison with the appreciably enlarged particle size of CSPNs stored in aqueous solution of pH 8.5 at 4 °C over 9 days (Fig. S3), the nearly unvaried size of H-PEG-CSPNs under the same storing condition was observed. Also, after being dispersed in 10 % FBS-containing PBS, the H-PEG-CSPNs maintained virtually unchanged particle size for 24 h (Fig. S4). Obviously, the highly hydrated mPEG corona of H-PEG-CSPNs could sufficiently promote their colloidal stability in aqueous phase, even in the presence of serum protein. Importantly, as presented in the ^{1}H-NMR spectrum of the acidity-treated H-PEG-CSPNs in DMSO-d_6 (Fig. S5), the disappearance of proton signals of the imine group at δ 8.5 ppm and the appearance of proton signals of the aldehyde group at δ 10.1 ppm strongly proved the acidity-elicited hydrolysis of the benzoic imine bonds between the chitosan and PEG. Undoubtedly, the H-PEG-CSPNs can detach outer PEG corona under weak acidic condition by cleavage of benzoic imine linkers. With the solution pH being adjusted from 7.4 to 5.0, in addition to conversion in zeta potential of H-PEG-CSPNs from −9.1 to +20.2 mV (Fig. 3b), their particle size was enlarged from 125 to 210 nm (Fig. 3f). This could be attributed to the following reasons. First, the acidity-elicited protonation of chitosan segments rendered the chitosan-rich shells of H-PEG-CSPNs massively positively charged. Second, the acidity-triggered hydrolysis of benzoic imine linkages led to detachment of mPEG-CHO from H-PEG-CSPNs, thus largely lowering π-π stacking and hydrophobic interaction within chitosan-constituted shells. As a result, the ionic osmotic pressure gradient was developed within positively-charged chitosan shells of nanomicelles to increase water inflow, thereby enabling nanomicelles to become swollen and loose. Such a considerable swelling of H-PEG-CSPNs in response to the pH reduction from 7.4 to 5.0 was also reflected by their increased R_g/R_h ratio from 0.773 to 0.887 (Fig. 3d and S6).

3.3. Preparation and characterization of DOX@PEG-CSPNs

Through one-pot co-assembly of PEGylated chitosan-g-PLGA adducts ([mPEG-CHO]/[chitosan-g-PLGA] = 2/3 (*w*/w)) and DOX molecules in aqueous solution of pH 8.5, the DOX molecules were encapsulated into H-PEG-CSPNs upon the π-π stacking and hydrophobic interaction to obtain DOX@H-PEG-CSPNs. For comparison, the co-association of DOX with chitosan-g-PLGA adducts, chitosan-g-PLGA/mPEG-CHO mixture, or PLGA/mPEG-CHO mixture at the same pH was conducted. Notably, as presented in Fig. 4a, massive precipitates were found in the above three control groups, while the well dispersion of DOX@H-PEG-CSPNs was observed. Evidently, in the lack of hydrophilic mPEG layer, the assemblies composed of DOX and chitosan-g-PLGA were apt to aggregate into huge precipitates. Furthermore, the simple physical mixing of mPEG-CHO segments with either chitosan-g-PLGA adducts or PLGA segments cannot endow the DOX-containing assemblies with the stable and hydrophilic mPEG layer, thus being incapable of avoiding inter-

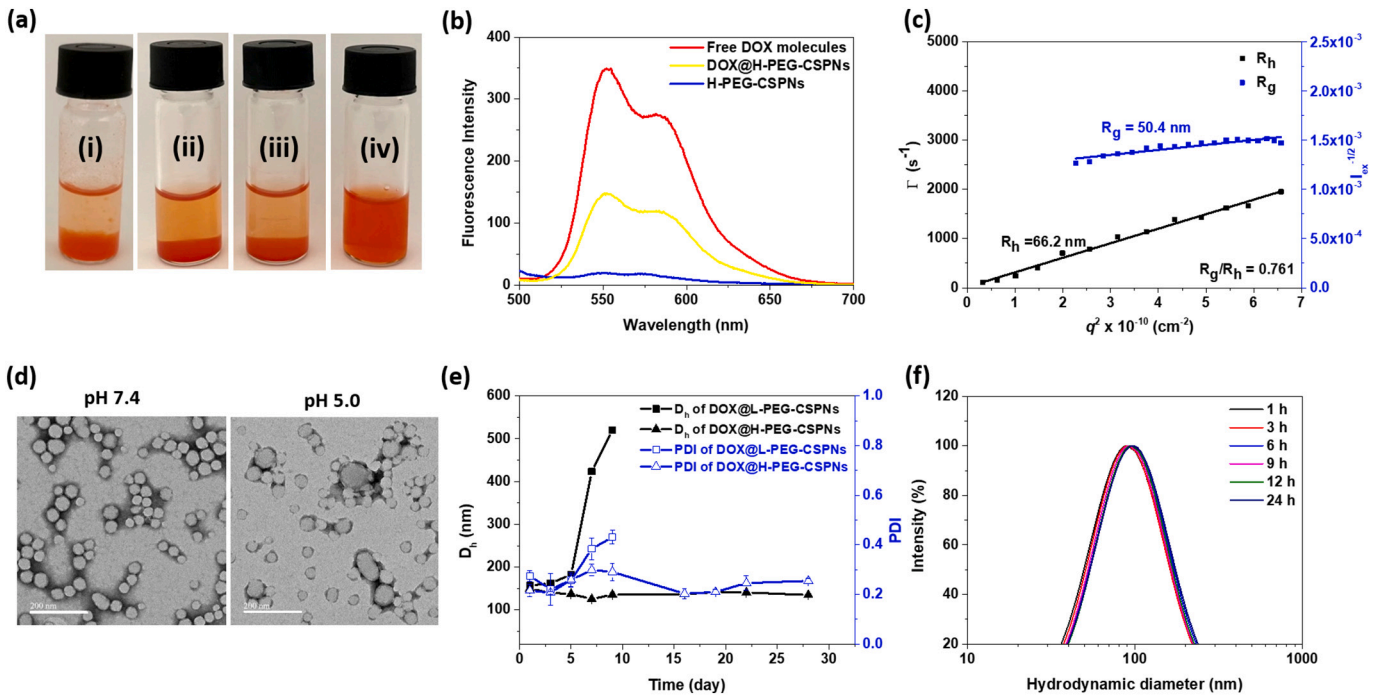

Fig. 4. (a) Optical photographs of (i) DOX/chitosan-g-PLGA assemblies, (ii) DOX/chitosan-g-PLGA/mPEG-CHO assemblies, (iii) DOX/PLGA/mPEG-CHO assemblies, and (iv) DOX@H-PEG-CSPNs in aqueous solutions at pH 7.4. (b) Fluorescence spectra of free DOX molecules, DOX@H-PEG-CSPNs and H-PEG-CSPNs in pH 7.4 PBS. (c) Berry plot for R_g and angle dependent correlation function of R_h of DOX@H-PEG-CSPNs in pH 7.4 PBS. (d) TEM images of DOX@H-PEG-CSPNs at pH 7.4 and 5.0. Scale bars are 200 nm. (e) Time-evolved mean D_h and PDI of DOX@H-PEG-CSPNs and DOX@L-PEG-CSPNs stored in aqueous solution of pH 8.5 at 4 °C. (f) DLS size distribution profiles of DOX@H-PEG-CSPNs in PBS containing 10 % FBS at different time intervals.

particle aggregation driven by hydrophobic interaction. Based on these findings, the use of as-synthesized PEGylated chitosan-g-PLGA adducts to co-associate with DOX molecules is a critical requirement for obtaining well-dispersed DOX-loaded nanoformulation. The drug loading efficiency and content of DOX@H-PEG-CSPNs were determined to be ca 76.5 % and 7.1 wt%, respectively (Table 1). Fig. 4b showed that the DOX fluorescence intensity of DOX@H-PEG-CSPNs was remarkably lower than that of free DOX molecules at the same drug concentration. This suggests that the high local concentration of DOX molecules entrapped within nanomicelles could give rise to marked fluorescence quenching of DOX [44]. As presented in Table 1, the DOX@H-PEG-CSPNs displayed a nano-scaled particle size (ca 137.8 nm) and monomodal size distribution (PDI 0.26). Moreover, in addition to a linear relationship between the relaxation frequency and the square of the scattering vector, the R_g/R_h value of DOX@H-PEG-CSPNs was attained to be ca 0.761 (Fig. 4c). The well-dispersed spherical shape of DOX@H-PEG-CSPNs at pH 7.4 was observed in their TEM images (Fig. 4d). These data illustrate that the DOX@H-PEG-CSPNs still retained onion-like core-shell-corona structure similar to drug-free H-PEG-CSPNs.

On the other hand, to explore the effects of PEGylation degree on the physicochemical properties of DOX-loaded nanomicelles, the DOX@L-PEG-CSPNs (with low PEGylation) were prepared. As presented in Table 1, the particle size (ca 162.3 nm) of DOX@L-PEG-CSPNs was appreciably larger than that (137.8 nm) of DOX@H-PEG-CSPNs. Moreover, the DOX@H-PEG-CSPNs exhibited a higher drug loading efficiency (76.5 %) as compared to DOX@L-PEG-CSPNs (62.5 %). Apparently, in comparison with low PEGylation level of DOX@L-PEG-CSPNs, the high PEGylation degree of DOX@H-PEG-CSPNs rendered their chitosan-rich shells more hydrophobic and compact due to formation of numerous benzoic imine bonds, thus reducing particle size and enhancing drug loading ability. Note that the DOX@H-PEG-CSPNs dispersed in aqueous solution of pH 8.5 stored at 4 °C for 28 days maintained nearly unvaried particle size and size distribution (Fig. 4e), whereas the DOX@L-PEG-CSPNs stored in the same environment beyond 5 days showed considerably enlarged particle size and size distribution, indicating the occurrence of inter-particle aggregation. Furthermore, it should be mentioned that the DOX@H-PEG-CSPNs dispersed in FBS-containing PBS at 37 °C retained virtually unchanged particle size over 24 h (Fig. 4f). No significant variation in the particle size of DOX@H-PEG-CSPNs suffered from large-volume dilution with pH 7.4 PBS was also observed (Fig. S7). These results strongly indicate that the high PEGylation level could equip DOX@H-PEG-CSPNs with outstanding colloidal stability and robust structure. Notably, when the solution pH was decreased from 7.4 to 5.0, in addition to shift in the zeta potential from −1.1 to +21.3 mV (Fig. 3b), the particle size of DOX@H-PEG-CSPNs was remarkably increased from 137.8 to 250.3 nm (Fig. 5a). Such an acidity-elicited size enlargement of DOX@H-PEG-CSPNs was also observed in their TEM images (Fig. 4d). Furthermore, the R_g/R_h value of DOX@H-PEG-CSPNs was changed from 0.761 to 0.884 in response to pH reduction from 7.4 to 5.0 (Fig. 5b). These findings indicate that the colloidal structure of DOX@H-PEG-CSPNs was transformed from dense to swollen state due to acidity-induced mPEG-CHO detachment and chitosan protonation (Scheme 1b). Similar pH-sensitive structural transformation was also attained for drug-free H-PEG-CSPNs.

In order to investigate the effects of pH-responsive structural transformation of DOX@H-PEG-CSPNs on drug liberation, the in vitro DOX release behavior at different pH was evaluated. As revealed in Fig. 5c, over a period of 24 h, the cumulative drug release of DOX@H-PEG-CSPNs was appreciably promoted from 31.8 to 48.5 % in response to pH adjustment from 7.4 to 4.0. Similar pH-responsive DOX liberation performance was also observed for DOX@L-PEG-CSPNs (Fig. S8). According to the aforementioned acidity-responsive structure change of DOX@H-PEG-CSPNs, it was concluded that the development of swollen and positively-charged chitosan shell as a result of acidity-triggered mPEG-CHO detachment and increased chitosan protonation, and the boosted repulsion force between the chitosan segments and protonated DOX molecules (pKa 8.6) facilitated DOX outflow from nanomicelles (Fig. 5d). Based on this finding, it is expected that the acidity-activated

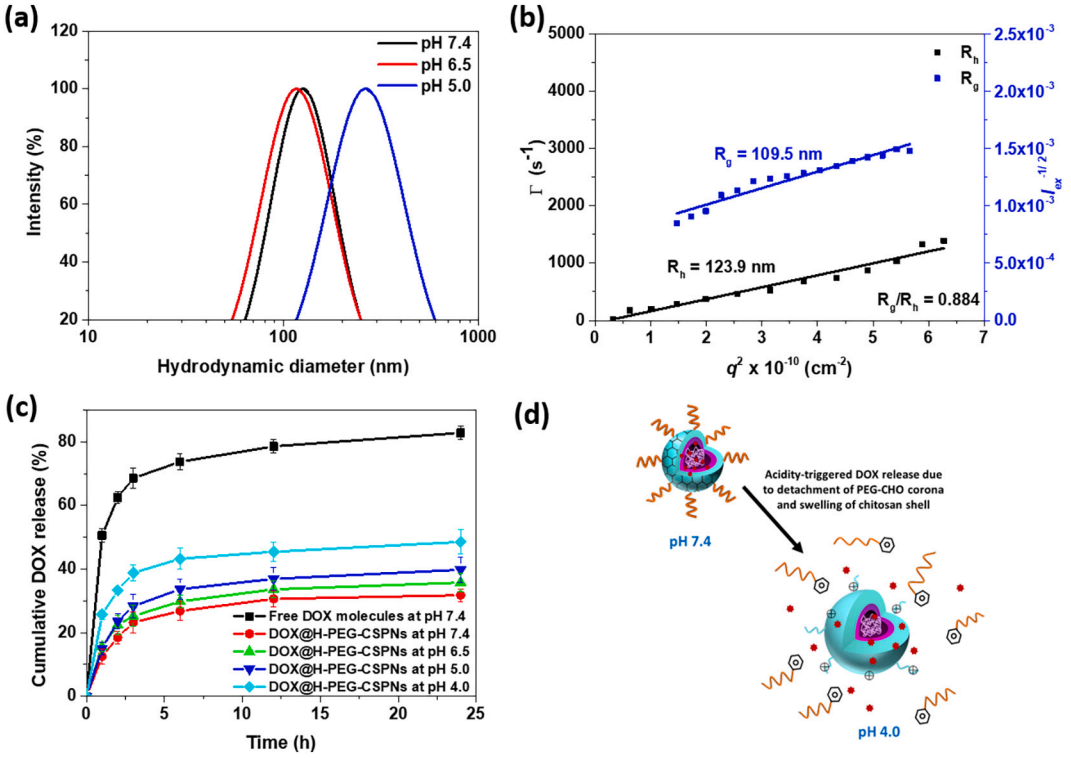

Fig. 5. (a) DLS particle size distribution profiles of DOX@H-PEG-CSPNs in aqueous solutions of different pH. (b) Berry plot for R_g and angle dependent correlation function of R_h of DOX@H-PEG-CSPNs in pH 5.0 acetate buffer. (c) Cumulative DOX release profiles of DOX@H-PEG-CSPNs in aqueous solutions of pH 7.4, 6.5, 5.0 and 4.0 at 37 °C. (d) Schematic illustration of acidity-responsive DOX release of DOX@H-PEG-CSPNs.

drug release of DOX@H-PEG-CSPNs within acidic endosomes and lysosomes of cancer cells could promote the transportation of DOX to cell nuclei for better anticancer efficacy.

3.4. *In vitro tumor acidity-mediated cellular internalization*

In the current study, as shown in the results of ^{1}H NMR, DLS and zeta potential measurements (Fig. S5, 5a and 3b), the DOX@H-PEG-CSPNs undergoing mPEG-CHO detachment and chitosan protonation in response to pH change from 7.4 to 6.5 still exhibited nearly unchanged particle size, but slightly positively-charged surfaces. More and more studies strongly demonstrate that the PEG detachment and positively-charged surface of nanoparticle-based drug delivery systems in tumor extracellular acidity and matrix can remarkably enhance their uptake by cancer cells [7,27–34]. In view of the above viewpoints, it is worth to explore the effects of pH_e-triggered mPEG-CHO detachment and surface charge conversion of DOX@PEG-CSPNs on the cellular uptake using TRAMP-C1 cells. As presented in the CLSM images (Fig. 6a), with 1-h incubation, DOX molecules delivered by DOX@H-PEG-CSPNs at pH 6.5 were markedly observed in the cytoplasm of TRAMP-C1 cells, whereas only few amounts of DOX transported by the counterparts at pH 7.4 were found intracellularly. Moreover, the DOX fluorescence intensity of TRAMP-C1 cells incubated with DOX@H-PEG-CSPNs for 1 h was considerably enhanced by around 1.4-fold with the culture pH being adjusted from 7.4 to 6.5 as shown in the flow cytometric histograms (Fig. 6b and c). Similar findings were also obtained for TRAMP-C1 cells treated with DOX@L-PEG-CSPNs at pH 7.4 and 6.5, respectively, for 1 h. Notably, with the incubation time being prolonged from 1 to 4 h, the accumulation of DOX delivered by DOX@H-PEG-CSPNs and DOX@L-PEG-CSPNs at pH 6.5 in the cytoplasm and nuclei of TRAMP-C1 cells was largely boosted as compared to that of the counterparts at pH 7.4 (Fig. 6a). Also, the flow cytometric data showed that the DOX fluorescence intensity of TRAMP-C1 cells treated with DOX@H-PEG-CSPNs and DOX@L-PEG-CSPNs at pH 6.5 was considerably increased by 1.79- and 1.75-fold, respectively, in response to the increase of incubation time from 1 to 4 h (Fig. 6b and c). By contrast, for TRAMP-C1 cells incubated with DOX@H-PEG-CSPNs and DOX@L-PEG-CSPNs, respectively, at pH 7.4, only 1.37- and 1.35-fold enhancement in the DOX fluorescence intensity was attained by prolonging incubation time. These findings evidently demonstrate that the cellular internalization of DOX@PEG-CSPNs in weak acidic milieu could be promoted by their enhanced affinity for cancer cells upon detachment of mPEG-CHO corona and exposure of positively-charged chitosan shell (Fig. 6d). Furthermore, when the incubation time was further prolonged, the cellular uptake of DOX@PEG-CSPNs in weak acidic environment was significantly augmented due to the increased dePEGylation degree, thereby considerably boosting DOX deposition within nuclei of TRAMP-C1 cells by intracellular DOX release of nanomicelles. Notably, the accumulation of free DOX molecules within nuclei of TRAMP-C1 cells was remarkably higher than that of DOX@PEG-CSPNs with high or low PEGylation degree. This could be ascribed to the different pathways of cellular uptake for free DOX molecules (passive diffusion) and nanomicelles (endocytosis) [45,46].

3.5. *In vitro chemotherapy*

Encouraged by the promoted internalization of DOX@PEG-CSPNs by TRAMP-C1 cells under mimic weak tumor extracellular environment, we evaluated their DOX-mediated anticancer efficacy on cancer cells. As an important control, TRAMP-C1 cells incubated with H-PEG-CSPNs (18.8–150 μg/mL) at pH 7.4 for 24 h retained the viability beyond 85 % (Fig. 7a), indicating the negligible toxicity of drug-free nanomicelles to cancer cells. When TRAMP-C1 cells were treated with free DOX molecules in the drug concentration range 0.63–10 μM, the cell viability was considerably declined with the increased DOX concentration (Fig. 7b), illustrating the cytotoxic effect of DOX. Note that the viability of TRAMP-C1 cells treated with DOX@H-PEG-CSPNs at pH 6.5 for 24 h was appreciably reduced in the DOX concentration-dependent manner

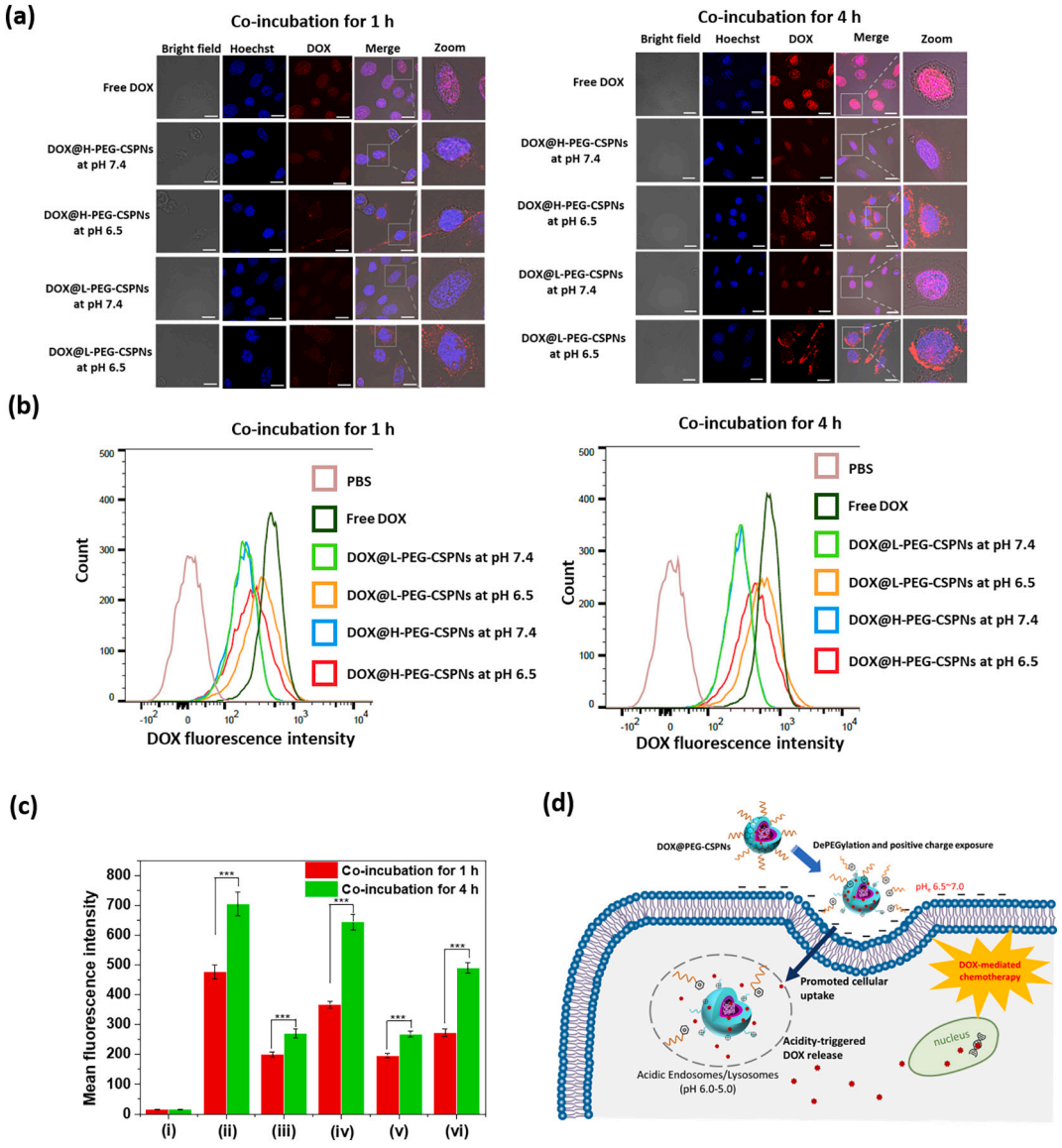

Fig. 6. (a) CLSM images of TRAMP-C1 cells incubated with free DOX molecules and DOX@H-PEG-CSPNs and DOX@L-PEG-CSPNs, respectively, at pH 7.4 and 6.5 for 1 and 4 h. (b) Flow cytometric histograms and (c) mean DOX fluorescence intensity of TRAMP-C1 cells incubated with (i) PBS, (ii) free DOX molecules at pH 7.4, (iii) DOX@L-PEG-CSPNs at pH 7.4, (iv) DOX@L-PEG-CSPNs at pH 6.5, (v) DOX@H-PEG-CSPNs at pH 7.4 and (vi) DOX@H-PEG-CSPNs at pH 6.5 for 1 and 4 h. (d) Schematic illustration of acidity-activated cellular uptake of DOX@PEG-CSPNs.

compared to that of TRAMP-C1 cells receiving the counterparts at pH 7.4 for 24 h (Fig. 7c). Moreover, the drug doses required for 50 % cellular growth inhibition (IC_{50}) value of DOX@H-PEG-CSPNs at pH 6.5 attained to be ca. 3.35 μM is significantly 2.6-fold lower than that (8.60 μM) of the counterparts at pH 7.4. Similar findings were also obtained with another cell model, 4 T1 cancer cells (Fig. S9). Furthermore, the fluorescence staining of live/dead TRAMP-C1 cells (Fig. 7d) revealed that most of TRAMP-C1 cells treated with DOX@H-PEG-CSPNs (DOX concentration: 0.63 μM) at pH 6.5 presented significant PI-positive staining in comparison with cells incubated with the counterparts at pH 7.4. Such an enhanced cytotoxicity of DOX@L-PEG-CSPNs incubated with TRAMP-C1 cells under weak acidic condition was also gained (Fig. S10). These results evidently suggest that the DOX@PEG-CSPNs could promote intracellular DOX delivery by means of acidity-triggered dePEGylation and positive charge exposure, thereby amplify the anticancer potency.

3.6. *In vivo tumor growth inhibition*

To evaluate the in vivo antitumor efficacy, the TRAMP-C1 tumor-bearing mice were treated, respectively, with free DOX molecules and DOX@PEG-CSPNs by intravenous injection. The tumor size and body weight of tumor-bearing mice were monitored every 2 days. The relative tumor volumes (V/V_o) were obtained by the normalization of the tumor volumes (V) against their original volumes (V_o). As presented in Fig. 8a, after 18 days post treatment, a considerable 17–22-fold increase in the relative tumor volume of mice treated with free DOX molecules was observed, being comparable with that of the mice received PBS. This indicates that free DOX molecules fail to suppress tumor growth because of the ineffective tumor accumulation of DOX. Similar results regarding the failure of free DOX molecules to hinder tumor growth were also reported elsewhere [47,48]. By contrast, during 18 days of treatment, the sound tumor growth inhibition was observed with DOX@PEG-CSPNs, particularly for DOX@H-PEG-CSPNs. As presented in Fig. 8b, tumors collected from the euthanized mice treated with DOX@H-PEG-

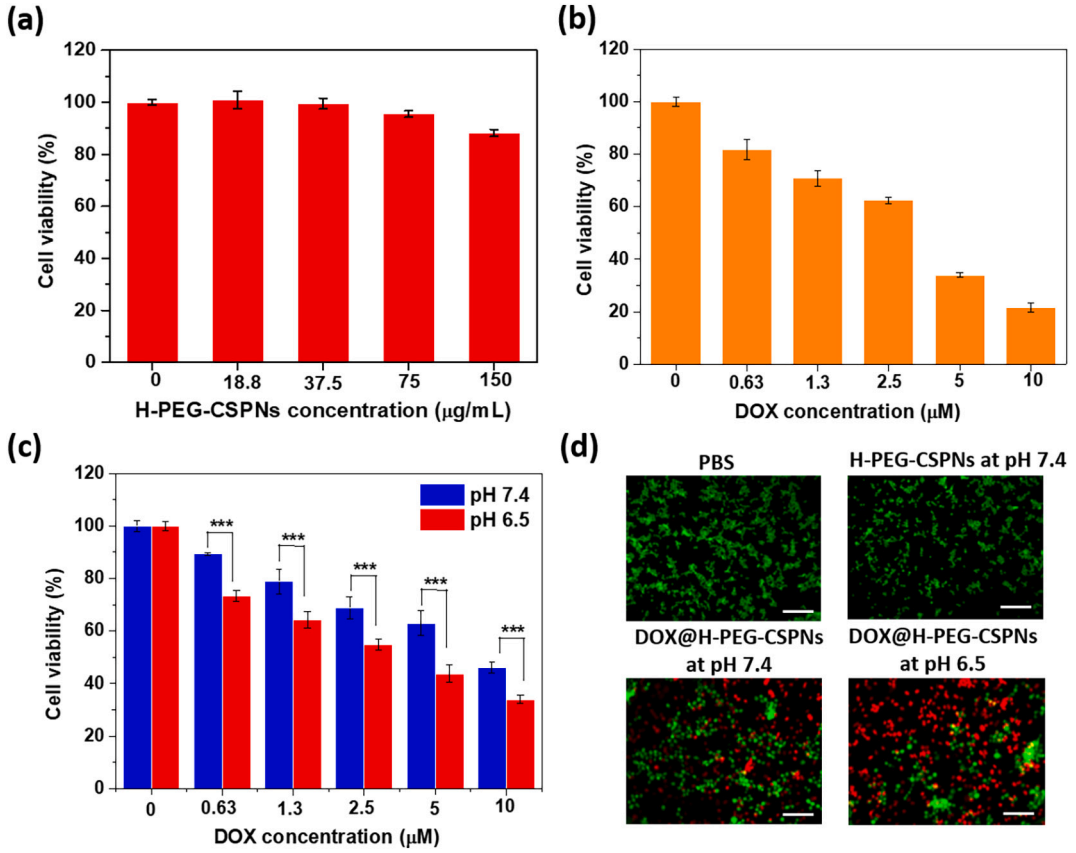

Fig. 7. Cell viability of TRAMP-C1 cells incubated with (a) H-PEG-CSPNs and (b) free DOX molecules, respectively, at 37 °C for 24 h. (c) Cell viability of TRAMP-C1 cells treated with DOX@H-PEG-CSPNs at pH 7.4 and 6.5, respectively, for 24 h. (d) Fluorescence images of TRAMP-C1 cells treated with PEG-CSPNs at pH 7.4, DOX@H-PEG-CSPNs (DOX concentration = 0.63 μM) at pH 7.4 and 6.5, respectively, at 37 °C for 24 h. The viable cells were stained green with Calcein AM, and the dead cells were stained red with PI. Scale bars are 200 μm.

CSPNs were the smallest among the tumors receiving other treatments, corresponding to the results of the in vivo tumor growth inhibition. Importantly, the average of TI (ca. 61.6 %) of DOX@H-PEG-CSPNs is appreciably higher than that (33.3 %) of DOX@L-PEG-CSPNs (Fig. 8c). Furthermore, as revealed in the H&E staining images of tumor sections (Fig. 8d), no significant necrosis was observed in the sections of both PBS and DOX groups, while nuclei shrinkage and cytoplasm leakage appeared in the sections of the other two DOX@PEG-CSPNs groups, particularly in the DOX@H-PEG-CSPNs group. Notably, the tumor sections of DOX@H-PEG-CSPNs group showed lowest Ki67 expression than those of other treatment groups, indicating their superior antiproliferative effects on xenograft tumors. In view of the above findings, it was demonstrated that the tumor acidity-induced dePEGylation of DOX@H-PEG-CSPNs accumulated in the tumor sites to expose their positively-charged chitosan-rich surfaces remarkably boosted the cellular uptake, thereby enhancing DOX-mediated antitumor effect (Scheme 1b). Moreover, it should be mentioned that the unsatisfied anticancer effect of DOX@L-PEG-CSPNs relative to DOX@H-PEG-CSPNs may be ascribed to their low PEGylation degree incapable of efficiently reducing their uptake by RES to achieve effective tumor-targeted drug delivery. On the other hand, the body weights of the treated mice in all groups had no considerable change, suggesting that the formulations employed in this study did not cause serious acute toxicity (Fig. 8e). Also, no significant tissue abnormality was attained in important organs including heart, liver, spleen, lung and kidney, of mice from all groups (Fig. S11).

4. Conclusions

In order to considerably enhance intracellular DOX delivery for better chemotherapy, the tumor-responsive H-PEG-CSPNs capable of detaching PEG shielding and exposing positively-charged chitosan surfaces were developed as DOX vehicles. Through self-assembly of amphiphilic benzoic imine-containing PEGylated chitosan-g-PLGA adducts in aqueous solution of pH 8.5, the H-PEG-CSPNs were fabricated and characterized to have a core-shell-corona spherical structure composed of a hydrophobic PLGA core surrounded by benzoic imine-rich chitosan shell and outer hydrophilic PEG corona. The PEG hydration and aromatic ring-containing chitosan shell of DOX@H-PEG-CSPNs endowed their excellent colloidal stability under large-volume dilution condition of PBS and in a serum-containing aqueous solution of physiological salt concentration. Notably, the DOX@H-PEG-CSPNs in weak acidic milieu displayed dePEGylation, surface charge conversion and accelerated drug liberation by the acidity-triggered cleavage of benzoic imine bonds and increased protonation of chitosan segments. The in vitro cellular uptake and cytotoxicity studies revealed that the cellular internalization of DOX@H-PEG-CSPNs under mimic tumor acidic condition by TRAMP-C1 cells was appreciably promoted by acidity-elicited detachment of PEG corona and exposure of positively-charged chitosan shell, thereby enhancing anticancer activity. The in vivo tumor growth suppression results revealed that the DOX@H-PEG-CSPNs inhibited TRAMP-C1 tumor growth superior to free DOX molecules and DOX@L-PEG-CSPNs, indicating their great promise to improve cancer therapy.

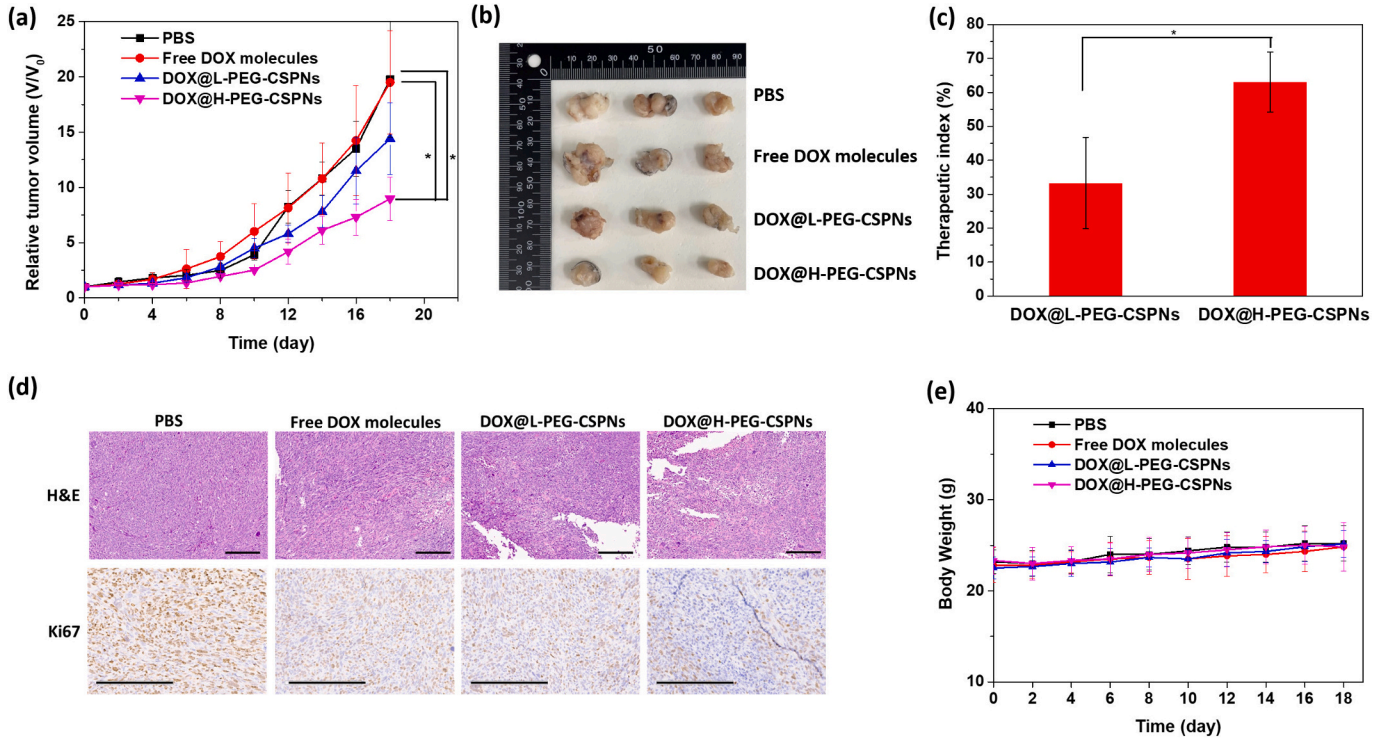

Fig. 8. (a) Tumor growth suppression profiles of TRAMP-C1 tumor-bearing mice receiving different formulations. (b) Photographs of the tumors of each group harvested from the euthanized mice at day 18 post the treatment. (c) TI value of DOX@L-PEG-CSPNs and DOX@H-PEG-CSPNs. (d) H&E staining and Ki67 staining images of tumor sections from TRAMP-C1 tumor-bearing mice receiving different treatments. Scale bars are 200 μm. (e) Body weight of TRAMP-C1 tumor-bearing mice injected with various formulations.

CRediT authorship contribution statement

Shih-Yu Huang: Conceptualization, Methodology, Investigation, Formal analysis. **Nien-Tzu Yeh:** Investigation, Validation, Resources. **Tzu-Hao Wang:** Investigation, Resources, Validation. **Tsai-Ching Hsu:** Methodology, Resources. **Hao-Yang Chin:** Methodology, Investigation. **Bor-Show Tzang:** Investigation, Resources, Funding acquisition, Supervision, Writing – review & editing. **Wen-Hsuan Chiang:** Conceptualization, Writing – original draft, Writing – review & editing, Supervision, Project administration, Funding acquisition.

Declaration of competing interest

The authors declare that they have no known competing financial interests or personal relationships that could have appeared to influence the work reported in this paper.

Data availability

Data will be made available on request.

Acknowledgments

This work is supported by the National Science and Technology Council (MOST 110-2628-E-005-001, and MOST 111-2628-E-005-009-MY2), National Chung Hsing University and Chung Shan Medical University (NCHU-CSMU 11101), Taiwan.

Appendix A. Supplementary data

Supplementary data to this article can be found online at https://doi.org/10.1016/j.ijbiomac.2022.12.172.

References

[1] B.N. Yalamandala, W.T. Shen, S.H. Min, W.H. Chiang, S.J. Chang, S.H. Hu, Advances in functional metal-organic frameworks based on-demand drug delivery systems for tumor therapeutics, Adv. NanoBiomed. Res. 1 (2021) 2100014.
[2] Y. Barenholz, Doxil®–the first FDA-approved nano-drug: lessons learned, J. Control. Release 160 (2012) 117–134.
[3] A.J. Montero, B. Adams, C.M. Diaz-Montero, S. Glück, Nab-paclitaxel in the treatment of metastatic breast cancer: a comprehensive review, Expert. Rev. Clin. Pharmacol. 4 (2011) 329–334.
[4] P. Wei, G. Gangapurwala, D. Pretzel, M.N. Leiske, L. Wang, S. Hoeppener, S. Schubert, J.C. Brendel, U.S. Schubert, Smart pH-sensitive nanogels for controlled release in an acidic environment, Biomacromolecules 20 (2019) 130–140.
[5] M. Mohammadi, L. Arabi, M. Alibolandi, Doxorubicin-loaded composite nanogels for cancer treatment, J. Control. Release 328 (2020) 171–191.
[6] S.J. Huang, T.H. Wang, Y.H. Chou, H.M. Wang, T.C. Hsu, J.L. Yow, B.S. Tzang, W. H. Chiang, Hybrid PEGylated chitosan/PLGA nanoparticles designed as pH-responsive vehicles to promote intracellular drug delivery and cancer chemotherapy, Int. J. Biol. Macromol. 210 (2022) 565–578.
[7] S. Wang, F. Zhang, G. Yu, Z. Wang, O. Jacobson, Y. Ma, R. Tian, H. Deng, W. Yang, Z.Y. Chen, X. Chen, Zwitterionic-to-cationic charge conversion polyprodrug nanomedicine for enhanced drug delivery, Theranostics 10 (2020) 6629–6637.
[8] X. Zhao, Y. Yao, K. Tian, T. Zhou, X. Jia, J. Li, P. Liu, Leakage-free DOX/PEGylated chitosan micelles fabricated via facile one-step assembly for tumor intracellular pH-triggered release, Eur. J. Pharm. Biopharm. 108 (2016) 91–99.
[9] F. Chai, L. Sun, X. He, J. Li, Y. Liu, F. Xiong, L. Ge, T.J. Webster, C. Zheng, Doxorubicin-loaded poly (lactic-co-glycolic acid) nanoparticles coated with chitosan/alginate by layer by layer technology for antitumor applications, Int. J. Nanomedicine 12 (2017) 1791–1802.
[10] M.J. Mitchell, M.M. Billingsley, R.M. Haley, M.E. Wechsler, N.A. Peppas, R. Langer, Engineering precision nanoparticles for drug delivery, Nat. Rev. Drug Discov. 20 (2021) 101–124.
[11] M. Zhang, X. Qin, Z. Zhao, Q. Du, Q. Li, Y. Jiang, Y. Luan, A self-amplifying nanodrug to manipulate the janus-faced nature of ferroptosis for tumor therapy, Nanoscale Horiz. 7 (2022) 198–210.
[12] X. Ren, N. Wang, Y. Zhou, A. Song, G. Jin, Z. Li, Y. Luan, An injectable hydrogel using an immunomodulating gelator for amplified tumor immunotherapy by blocking the arginase pathway, Acta Biomater. 124 (2021) 179–190.
[13] D. Guimarães, A. Cavaco-Paulo, E. Nogueira, Design of liposomes as drug delivery system for therapeutic applications, Int. J. Pharm. 601 (2021), 120571.
[14] Y. Liu, K.M. Castro Bravoa, J. Liu, Targeted liposomal drug delivery: a nanoscience and biophysical perspective, Nanoscale Horiz. 6 (2021) 78–94.

[15] Y. Wang, A. Khan, Y. Liu, J. Feng, L. Dai, G. Wang, N. Alam, L. Tong, Y. Ni, Chitosan oligosaccharide-based dual pH responsive nano-micelles for targeted delivery of hydrophobic drugs, Carbohydr. Polym. 223 (2019), 115061.
[16] M. Ghezzi, S. Pescina, C. Padula, P. Santi, E. Del Favero, L. Cantù, S. Nicoli, Polymeric micelles in drug delivery: An insight of the techniques for their characterization and assessment in biorelevant conditions, J Control Release 332 (2021) 312–336.
[17] Y. Dai, X. Chen, X. Zhang, Recent advances in stimuli-responsive polymeric micelles via click chemistry, Polym. Chem. 10 (2019) 34–44.
[18] L. Xu, X. Wang, Y. Liu, G. Yang, R.J. Falconer, C.X. Zhao, Lipid nanoparticles for drug delivery, Adv. NanoBiomed Res. 2 (2022) 2100109.
[19] V. Mishra, K.K. Bansal, A. Verma, N. Yadav, S. Thakur, K. Sudhakar, J. M. Rosenholm, Solid lipid nanoparticles: emerging colloidal nano drug delivery systems, Pharmaceutics 10 (2018) 191.
[20] J. Cao, X. Li, H. Tian, Metal-organic framework (MOF)-based drug delivery, Curr. Med. Chem. 27 (2020) 5949–5969.
[21] M. Falsafi, A.Sh. Saljooghi, K. Abnous, S.M. Taghdisi, M. Ramezani, M. Alibolandi, Smart metal organic frameworks: focus on cancer treatment, Biomater. Sci. 9 (2021) 1503–1529.
[22] Q.S. Wang, L.N. Gao, X.N. Zhu, Y. Zhang, C.N. Zhang, D. Xu, Y.L. Cui, Co-delivery of glycyrrhizin and doxorubicin by alginate nanogel particles attenuates the activation of macrophage and enhances the therapeutic efficacy for hepatocellular carcinoma, Theranostics 9 (2019) 6239–6255.
[23] L. Kong, F. Campbell, A. Kros, DePEGylation strategies to increase cancer nanomedicine efficacy, Nanoscale Horiz. 4 (2019) 378–387.
[24] J.S. Suk, Q.G. Xu, N. Kim, J. Hanes, L.M. Ensign, PEGylation as a strategy for improving nanoparticle-based drug and gene delivery, Adv. Drug Deliv. Rev. 99 (2016) 28–51.
[25] J.M. Harris, R.B. Chess, Effect of pegylation on pharmaceuticals, Nat. Rev. Drug Discov. 2 (2003) 214–221.
[26] F.M. Veronese, G. Pasut, PEGylation, successful approach to drug delivery, Drug Discov. Today 10 (2005) 1451–1458.
[27] Y.H. Chou, Y.L. Liu, T.C. Hsu, J.L. Yow, B.S. Tzang, W.H. Chiang, Tumor acidity-responsive polymeric nanoparticles to promote intracellular delivery of zoledronic acid by PEG detachment and positive charge exposure for enhanced antitumor potency, J. Mater. Chem. B 10 (2022) 4363–4374.
[28] Z. Yang, N. Sun, R. Cheng, C. Zhao, Z. Liu, X. Li, J. Liu, Z. Tian, pH multistage responsive micellar system with charge-switch and PEG layer detachment for co-delivery of paclitaxel and curcumin to synergistically eliminate breast cancer stem cells, Biomaterials 147 (2017) 53–67.
[29] Z. Jiang, X. Feng, H. Zou, W. Xu, X. Zhuang, Poly(L-glutamic acid)-cisplatin nanoformulations with detachable PEGylation for prolonged circulation half-life and enhanced cell internalization, Bioact. Mater. 6 (2021) 2688–2697.
[30] X. Li, S.A. Valdes, R.F. Alzhrani, S. Hufnagel, S.D. Hursting, Z. Cui, Zoledronic acid-containing nanoparticles with minimum premature release show enhanced activity against extraskeletal tumor, ACS Appl. Mater. Interfaces 11 (2019) 7311–7319.
[31] M.H. Hsieh, T.H. Wang, S.H. Hu, T.C. Hsu, J.L. Yow, B.S. Tzang, W.H. Chiang, PEGylated chitosan/folate-decorated polydopamine nanoparticles to augment antitumor efficacy of photothermal/chemo combination therapy, Chem. Eng. J. 446 (2022), 137243.
[32] Q. Chen, C. Jia, Y. Xu, Z. Jiang, T. Hu, C. Li, X. Cheng, Dual-pH responsive chitosan nanoparticles for improving in vivo drugs delivery and chemoresistance in breast cancer, Carbohydr. Polym. 290 (2022), 119518.
[33] X. Xu, J. Duan, Q. Lan, Y. Kuang, T. Liao, Y. Liu, Z. Xu, J. Chen, B. Jiang, C. Li, A dual-sensitive poly(amino acid)/hollow mesoporous silica nanoparticle-based anticancer drug delivery system with a rapid charge-reversal property, J. Drug Deliv. Sci. Technol. 66 (2021), 102817.
[34] C.C. Hung, W.C. Huang, Y.W. Lin, T.W. Yu, H.H. Chen, S.C. Lin, W.H. Chiang, H. C. Chiu, Active tumor permeation and uptake of surface charge-switchable theranostic nanoparticles for imaging-guided photothermal/chemo combinatorial therapy, Theranostics 6 (2016) 302–317.
[35] L. Li, P. Zhang, C. Li, Y. Guo, K. Sun, In vitro/vivo antitumor study of modified-chitosan/carboxymethyl chitosan "boosted" charge-reversal nanoformulation, Carbohydr. Polym. 269 (2021), 118268.
[36] Y. Mu, G. Wu, C. Su, Y. Dong, K. Zhang, J. Li, X. Sun, Y. Li, X. Chen, C. Feng, pH-sensitive amphiphilic chitosan-quercetin conjugate for intracellular delivery of doxorubicin enhancement, Carbohydr. Polym. 223 (2019), 115072.
[37] X. Song, J. Wang, Y. Xu, H. Shao, J. Gu, Surface-modified PLGA nanoparticles with PEG/LA-chitosan for targeted delivery of arsenic trioxide for liver cancer treatment: inhibition effects enhanced and side effects reduced, Colloids Surf. B Biointerfaces. 180 (2019) 110–117.
[38] M. Alibolandi, S.Amel Farzad, M. Mohammadi, K. Abnous, S.M. Taghdisi, F. Kalalinia, M. Ramezani, Tetrac-decorated chitosan-coated PLGA nanoparticles as a new platform for targeted delivery of SN38, Artif. Cells Nanomed. Biotechnol. 46 (2018) 1003–1014.
[39] S.C. Liao, C.W. Ting, W.H. Chiang, Functionalized polymeric nanogels with pH-sensitive benzoic-imine cross-linkages designed as vehicles for indocyanine green delivery, J. Colloid Interface Sci. 561 (2020) 11–22.
[40] D. Sprouse, Y. Jiang, J.E. Laaser, T.P. Lodge, T.M. Reineke, Tuning cationic block copolymer micelle size by pH and ionic strength, Biomacromolecules 17 (2016) 2849–2859.
[41] V.T.A. Nguyen, M.D. Pauw-Gillet, O. Sandre, M. Gauthier, Biocompatible polyion complex micelles synthesized from arborescent polymers, Langmuir 32 (2016) 13482–13492.
[42] Y. Guo, S.W. Hui, Poly(ethylene glycol)-conjugated surfactants promote or inhibit aggregation of phospholipids, Biochim. Biophys. Acta Biomembr. 1323 (1997) 185–194.
[43] J. Wu, S. Chen, Investigation of the hydration of nonfouling material poly(ethylene glycol) by low-field nuclear magnetic resonance, Langmuir 28 (2012) 2137–2144.
[44] N.S. Elbialy, N. Mohamed, Alginate-coated caseinate nanoparticles for doxorubicin delivery: preparation, characterization, and in vivo assessment, Int. J. Biol. Macromol. 154 (2020) 114–122.
[45] X.T. Shuai, H. Ai, N. Nasongkla, S.J. Kim, J.M. Gao, Micellar carrier based on block copolymers of poly(ε-caprolactone) and poly(ethylene glycol) for doxorubicin delivery, J. Control. Release 98 (2004) 415–426.
[46] M. Ishii, Y. Fukuoka, S. Deguchi, H. Otake, T. Tanino, N. Nagai, Energy-dependent endocytosis is involved in the absorption of indomethacin nanoparticles in the small intestine, Int. J. Mol. Sci. 20 (2019) 476.
[47] T. Liao, C. Liu, J. Ren, H. Chen, Y. Kuang, B. Jiang, J. Chen, Z. Sun, C. Li, A chitosan/mesoporous silica nanoparticle-based anticancer drug delivery system with a "tumor-triggered targeting" property, Int. J. Biol. Macromol. 183 (2021) 2017–2029.
[48] C.Y. Sun, Z. Cao, X.J. Zhang, R. Sun, C.S. Yu, X. Yang, Cascade-amplifying synergistic effects of chemo-photodynamic therapy using ROS-responsive polymeric nanocarriers, Theranostics 8 (2018) 2939–2953.